Temperature-insensitive fiber cantilever vibration sensor based on a fiber-to-fiber structure

Ben Xu (徐 贲)[1], Jianqing Li (李建庆)[1*], Yuanyuan Pan (潘媛媛)[1], Yi Li (李 裔)[2], and Xinyong Dong (董新永)[2]

[1]*Faculty of Information Technology, Macau University of Science and Technology, Avenida Wai Long, Taipa 999078, Macao SAR, China*

[2]*College of Optical and Electronic Technology, China Jiliang University, Hangzhou 310018, China*

[*]*Corresponding author: jqli@must.edu.mo*

Received October 19, 2013; accepted December 19, 2013; posted online January 27, 2014

A simple optical fiber cantilever vibration sensor consisting of two opposite aligned bare optical fibers sealed in a quartz capillary is presented.The fiber with the longer bare section is suspended in air and acts as a cantilever. By detecting the transmission power of the sensor directly, the environmental vibrational frequencies and amplitudes may be obtained. By adjusting the cantilever's natural deflection angle, the sensor can achieve high sensitivity, good response linearity, and a wide dynamic range. Coupling conditions are optimized to minimize temperature effects by simply setting an appropriate air gap between the bare fibers.

OCIS codes: 060.2370,280.4788, 120.7280.
doi: 10.3788/COL201412.020604.

Optical fiber vibration sensors have been studied extensively because of their intrinsic features which include non-conductivity, immunity to electromagnetic interference, and high sensitivity; such properties render these sensors favorable for use in conductive, erosive, or explosive environments.

Most fiber optic vibration sensors are based on interferometers or fiber Bragg gratings (FBGs). Interferometric sensors[1−7] are susceptible to phase noise because of random fluctuations in the fiber length caused mainly by temperature differences along the fiber. To reduce the effects of temperature and other low-frequency environmental noise on the detected signals, a feedback loop circuit is usually used as a comparator to generate the desired quadrature condition[8,9]. Temperature compensation is also necessary in FBG-based sensors[10−14]. Optical filters are an essential demodulation component of FBG-based vibration-sensing systems[12,15−19]. For these two types of vibration sensors, both temperature compensation techniques and optical filters increase the complexity and cost of sensors.

Besides the sensors described above, another type of fiber vibration sensor based on direct light power measurement has recently been proposed. Su *et al.*[20] reported a micro cantilever sensor based on an aligned fiber-to-tip structure for acoustic vibration sensing. In this sensor, a fiber tip with an aperture of tens of nanometers was made using a CO_2 laser-tapering system and stabilized on a high-resolution piezostage to align with a single-mode fiber (SMF). The coupled light power emanating from the SMF to the tapered fiber tip was then modulated by lateral displacement of the tip induced by vibrations. This microcantilever sensor can detect displacement at the micron level, but fabrication of the tip and package of the sensor is complex and difficult because of rigorous alignment conditions. Trudel *et al.*[21] studied a one-dimensional SMF displacement sensor that was also based on waveguide alignment. This sensor had a simple fiber-to-fiber structure (FFS) and a maximum displacement sensitivity of 2.46 dB/μm within a range of over 20 μm. However, despite their significant contributions to the topic, these previous studies[20,21] neither discuss the elements that affect sensor performance nor demonstrate how to optimize them.

In this study, we propose a vibration sensor based on a structure similar to that described in previous works. Two aligned bare optical fibers are sealed in a quartz capillary to protect them from dust and water and for easier employment in harsh environments. We investigate how the axial pre-offset (Δy) and air gap (l) between the two fibers influence the sensitivity, response linearity, and dynamic range of the sensor. Simulation results show that natural deflection of the fiber cantilever is crucial to improve the sensitivity of the device. More importantly, based on this natural deflection, we discuss optimal coupling conditions to alleviate the effects of temperature on the detected signals by simply setting an appropriate l between fibers.

Figure 1 shows a schematic diagram and microscopy images of the proposed vibration sensor. As shown in Fig. 1(a), two SMFs (SMF-28, Corning, USA) are inserted into a quartz capillary with an inner diameter of 250±3 μm and a narrow l between the free ends to form an FFS. The SMF with the shorter suspended bare section acts as the emitting fiber, while the SMF with the longer suspended section acts as the receiving fiber. Considering that the inner diameter of the capillary is nearly equal to the diameter of the fiber jacket (245±5 μm) and larger than that of the bare fiber (125.0 ±0.7μm), the capillary not only holds and aligns the two fibers but also allows the receiving fiber to function as a cantilever that may be subjected to environmental vibrations. The capillary further forms a suitable package that protects the sensor from dust and water. Vibrations may be

simply detected by directly measuring the transmission power of the sensor. Compared with existing cantilever sensors based on optical waveguide alignment[22,23], this capillary packaging does not require multidimensional and rigorous alignment and offers the advantages of easy fabrication, low cost, and robustness.

Figure 1(b) shows that the l between the emitting and receiving SMFs is approximately 160 μm. The two ends of the capillary are designed with tapered apertures for easy insertion and gluing of the two SMFs, as shown in Fig. 1(c).

We investigate which elements affect sensor performance based on theoretical simulations. Figure 2 shows the theoretical coupled power of the FFS described in Fig. 1 versus the lateral displacement d between the two fiber ends for different l obtained using a wide-angle beam propagation method with a Padé (4, 4) approximate operator and perfectly matched layer boundary conditions[24]. As the lateral displacement increases, the optical power received by the right fiber decreases monotonously. When the FFS is subjected to vibrations, the left emitting fiber maybe assumed to remain undeformed (as analyzed in the following text) whereas the right fiber cantilever is deformed. The received optical power is thus modulated by oscillations induced by vibrations.

To achieve linear responses and maximum d sensitivity, d must be correctly set. The weight of the fiber cantilever induces a small d called the natural pre-offset,

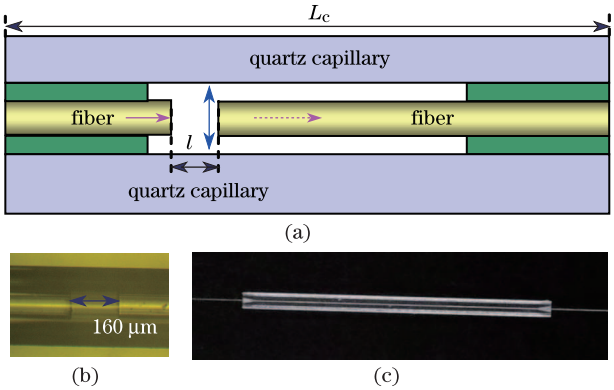

Fig. 1. (Color online) (a) Schematic diagram of the proposed sensor; (b) microscopic image of the air gap of the FFS; (c) photo of the packaged sensor.

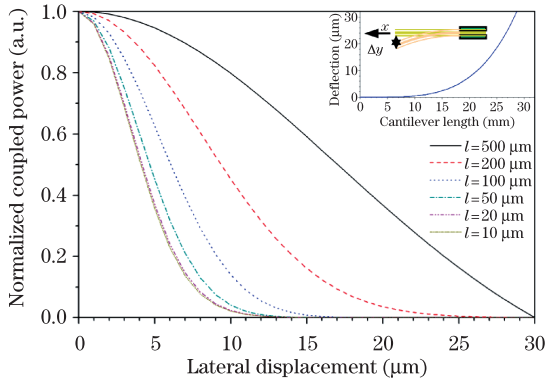

Fig. 2. (Color online) Calculated results of the coupled power of the FFS different air gaps. Here, the y-axis is normalized by the maximal coupled power with a lateral displacement of zero.

Δy. This Δy may be evaluated by using the formula[25]:

$$\Delta y = WL^3/8EI, \quad (1)$$

where L is the length of the fiber cantilever, W is the weight of the fiber cantilever ($W = \pi\rho D^2 Lg/4$, where ρ is the mass density of the bare fiber at $\sim$2.65×10^3 kg·m^{-3}, D is the diameter at $\sim$125 μm, and g is the gravitational acceleration at $\sim$9.8 N·kg^{-1}), E is the elastic modulus of the beam at $\sim$7.0×10^{10} kg·s^{-2}, and I is the moment of inertia of the beam cross-section (for a circular cross-section, $I = \pi D^4/64$). The inset in Fig. 2 shows the theoretical Δy versus L. The Δy can be adjusted by controlling the length of the right fiber cantilever. In other words, the Δy may be utilized to induce the sensor to operate in the linear portion of the coupling curve with high sensitivity as long as the cantilever is of the appropriate length.

Given that the maximum value of Δy is limited by the inner diameter of the capillary, the L of the right bare fiber is limited correspondingly, although a longer cantilever leads to stronger responses to external vibrations. In our experiments, the L values of the emitting and receiving fibers of our sensor were set to approximately 1 and 17 mm, respectively, and their corresponding Δy values were approximately 5×10^{-5} and 4 μm, respectively. Therefore, deformation of the left emitting fiber can be neglected. Considering the uncertainties of the fiber and inner capillary diameters, the total Δy may reach up to 10 μm, which means the dynamic range of d must be wide enough. Values of l may be adjusted according to Fig. 2, although lower d sensitivity may arise. When l <20 μm, the dynamic range of d is only about 10 μm, which is close to the Δy, and the plot of P versus d does not vary significantly. This finding suggests that l must be >20 μm. Similar sensors previously reported in Refs. [22,23] have alignment tolerances of only several micrometers. This feature allows easy fabrication of the proposed sensor without rigorous alignment requirements.

The temperature sensitivity of the transmission power of the sensor, S_T, can be expressed as

$$S_T = \mathrm{d}P/\mathrm{d}T = \mathrm{d}P/\mathrm{d}l \cdot \mathrm{d}l/\mathrm{d}T \approx S_l \cdot (\Delta\alpha \cdot L_c), \quad (2)$$

where P, T, and l denote the output light power, temperature, and length of the air gap, respectively; S_l denotes the sensitivity of the coupled light power to l; L_c is the length of capillary; $\Delta\alpha$ is the difference between the thermal expansion coefficients of the quartz capillary and optical fibers. S_T is obviously directly proportional to S_l that can be caculated based on the simulation results shown in Fig. 3.

Figure 3 shows the calculated results of P versus l for different Δy. When calculating P, the slope of the end face of the fiber cantilever is neglected because d is only approximately several micrometers, much shorter than the length of the cantilever. The calculated P first increases and then subsequently decreases with decreasing l for a given Δy, as proven by the experimental results. Figure 3 also demonstrates that the change trend of the measured transmission light power matches that of the calculation results. The margin between the experimental and calculation results is further illustrated in Fig. 3. This margin can be explained in two ways: On the one

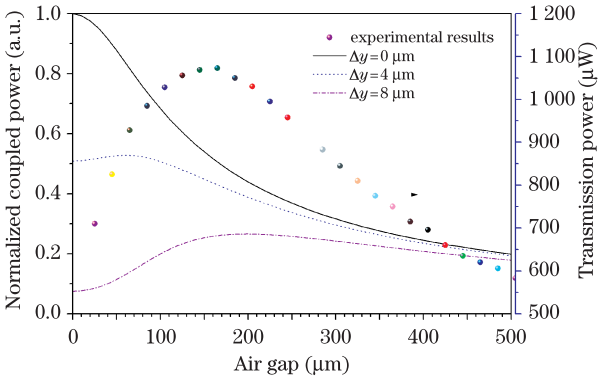

Fig. 3. (Color online) The coupled power of the proposed sensor versus the length of the air gap. Here, the left y-axis is normalized by the power launched from the fixed end of the short fiber. The balls denote the measured power, and the solid and dashed lines denote the calculated powers.

hand, the experimental data use absolute powers corresponding to the right y-axis and the calculation results use normalized powers corresponding to the left y-axis. On the other hand, the real Δy in our experiments is not exactly equal to the theoretical Δy based on Eq. (1) because of the uncertainty of the jacket diameter and the inner diameter of the quartz capillary. The trend of transmission light power implies that S_l is lowest when P reaches maximum. This feature allows us to alleviate the S_T by simply setting an appropriate l that can be achieved by monitoring the output power of the sensor during the adjustment process. The maximum P may be attributed to the Δy and the cone distribution of the optical field generated by the emitting fiber.

A vibration sensor was fabricated with a 17-mm fiber cantilever. The transmission light power of this sensor first increases and subsequently decreases with decreasing l, as may be expected from Fig. 3 (balls denote the experimental data). Based on our theoretical analysis of the temperature effects presented above, the l was finally set to approximately 160 μm, corresponding to the maximum output power.

An experimental setup similar to that described in Ref. [8] was constructed. A laser with a wavelength of 1,550 nm was used as a light source. This sensor was attached to a square metal plate by gluing of the capillary to it. A speaker was used as the vibration source. Light from the laser was coupled to the sensor, and the output power of the sensor was detected by an InGaAs photodetector. The electronic signals were then collected by a data acquisition card. Finally, the time domain power signal was converted to a frequency spectrum through fast Fourier transform. A LabVIEW program was developed to control data collection and processing.

Considering the large Δy and l in our experiments, no obvious Fabry–Pérot interference fringes are observed in the transmission spectrum of the sensor. Figure 4 shows a power spectrum and the corresponding time domain sensor signal output when the speaker is driven by 5-V, 2-kHz sinusoidal voltages. The output power of the sensor varies with uniform amplitude, and the demodulated frequency agrees well with that of the electric signal; here, a signal-to-noise ratio (SNR) of approximately 81.7 dB is observed. The corresponding harmonics of the induced vibration frequency were also observed. Harmonics may be explained by the principle of Fourier transform, where a discrete periodical signal (i.e., the measured transmission light intensity, which is discrete because of the limited sampling frequency) may be expanded as a fundamental frequency signal and a series of its harmonic frequency signals[26]. The tone of the fundamental frequency overwhelms the second, third, and fourth harmonics with differences of 20.1, 28.5, and 41.0 dB, respectively; these differences allow us to clearly identify the vibration frequency.

Figure 5 shows the amplitude responses of the FFS to vibrations driven by a 1 kHz sinusoidal wave at different voltages; the inset shows details of the measured signals at driving voltages of 0.5, 2.5, and 5 V. The amplitude of output power is linear to the drive signal amplitude, which implies that estimation of the vibration amplitude based on the output power of the sensor is possible. The results prove the positive effect of the natural Δy of the cantilever on the operation of the sensor in the linear portion of the coupling curve, as analyzed previously.

To prove the temperature insensitivity of our sensor, the vibration sensor with the speaker and metal plate was placed in a thermostat. The static transmission light intensities of the sensor are 0.02478, 0.02453, 0.02439, and 0.02366 at 10, 20, 30, and 40 °C, respectively. As expected, the variation of intensity versus the temperature can be neglected. Figure 6 shows the responses of the sensor to a speaker driven by a 5-V, 1-kHz sinusoidal wave at different temperatures. The amplitude of the

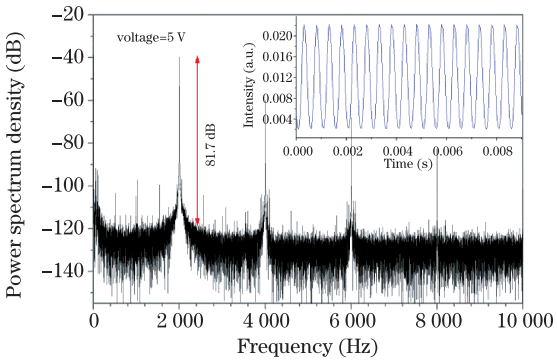

Fig. 4. (Color online) Frequency responses of the proposed sensor to vibrations driven by 5-V, 2-kHz sinusoidal voltages. Inset: time domain responses.

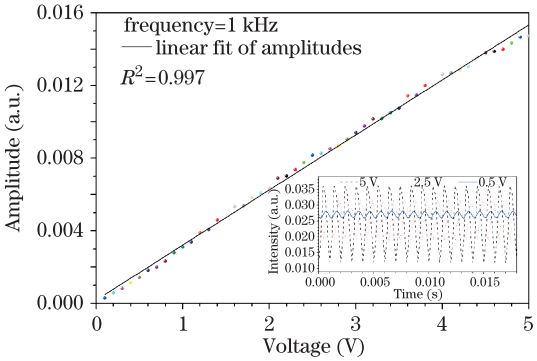

Fig. 5. (Color online) Amplitude responses of the proposed sensor to vibrations driven by 1-kHz sinusoidal voltages. Inset: time domain responses at 0.5, 2.5, and 5 V.

transmission light intensity varies slightly as the temperature changes by nearly 30 °C, as shown in Fig. 6(a). All of the measured vibration frequencies agree with the acoustic source frequency equaling 1 kHz. The SNR varies slightly, as shown in Fig. 6(b), where each of the frequency ranges from 500 to 1,500 Hz for four temperatures. These test results imply that the sensor allows stable performance despite fluctuations in temperature.

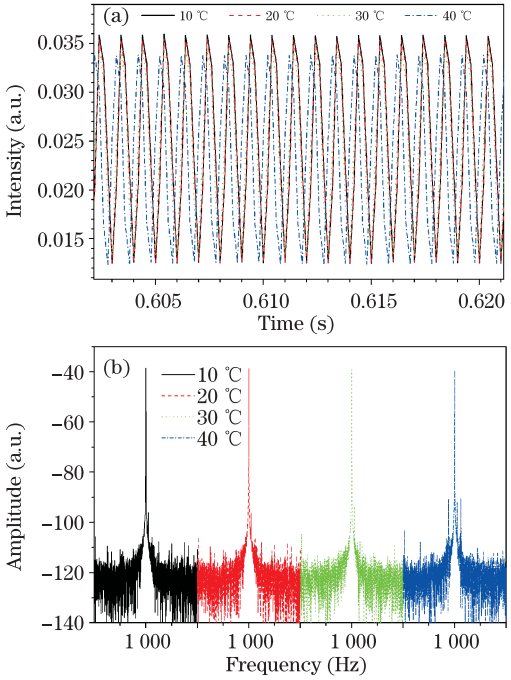

Fig. 6. (Color online) Responses of the sensor to a speaker driven by 5-V, 1-kHz sinusoidal voltages at different temperatures in the (a) time and (b) corresponding frequency domains.

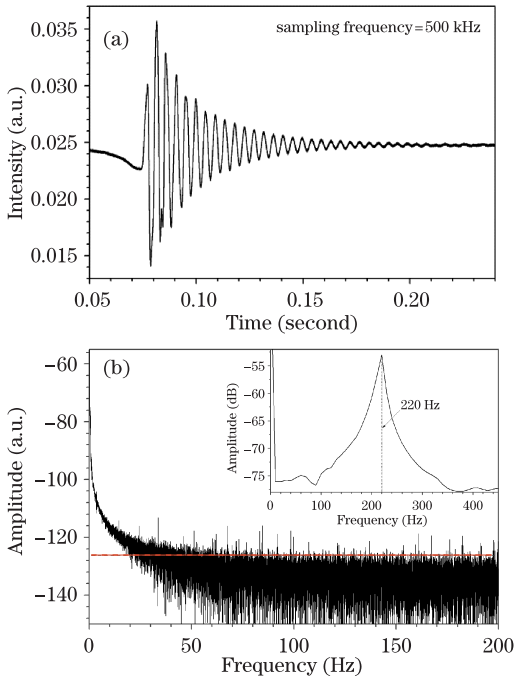

Fig. 7. (Color online) Impulse responses of the sensor in the (a) time and (b) corresponding frequency domains. The red dashed line represents the background level. Inset: responses within the low-frequency range.

Finally, Fig. 7 shows the impulse responses of the sensor measured by pressing the metal plate until it sinks appreciably and releasing it to allow free oscillation. A perfectly damped oscillation waveform in the time domain with a sampling frequency of 500 kHz is shown in Fig. 7(a); the corresponding response in the frequency domain is shown in Fig. 7(b). The red line indicates the background level. The sensor has a wide frequency response range spanning a few hertz to tens of kilohertz. The inset in Fig. 7(b) shows sensor responses within the low-frequency range. The frequency with maximum amplitude is the resonance frequency of the sensor and equals 220 Hz.

In conclusion, we discuss and optimize a FFS vibration sensor from the theoretical and experimental aspects. The sensor is extremely easy to construct with only one-dimensional adjustment and may be packaged in a quartz capillary. Our theoretical analysis and experiments show that the natural deflection of the fiber cantilever induced by its own weight can be used to obtain higher sensitivity, better response linearity, and wider dynamic ranges. The effects of temperature on the sensor can be alleviated by simply setting an optimum l between the two bare fibers for any given Δy. The optimized sensor is fairly reliable on the premise that the fiber cantilever does not vibrate with large amplitudes limited by the inner diameter of the quartz capillary.

This work was supported by the Science and Technology Development Fund, Macao SAR, China (No. 082/2012/A3), the National Natural Science Foundation of China (No. 61007051), and the Qianjiang Talent Program of Zhejiang Province, China (No. QJD1302016).

References

1. Y. Li, X. Wang, and X. Bao, Appl. Opt. **50,** 1873 (2011).
2. Q. Sun, D. Liu, J. Wang, and H. Liu, Opt. Commun. **281,** 1538 (2008).
3. X. Hong, J. Wu, C. Zuo, F. Liu, H. Guo, and K. Xu, Appl. Opt. **50,** 4333 (2011).
4. K. A. Murphy, M. F. Gunther, A. M. Vengsarkar, and R. O. Claus, Opt. Lett. **16,** 273 (1991).
5. F.C. Favero, L. Araujo, G. Bouwmans, V. Finazzi, J. Villatoro, and V. Pruneri, Opt. Express **20,** 7112 (2012).
6. K. Wada, H. Narui, D. Yamamoto, T. Matsuyama, and H. Horinaka, Opt. Express **22,** 21467 (2011).
7. F. Peng, J. Yang, B. Wu, Y. Yuan, X. Li, A. Zhou, and L. Yuan, Chin. Opt. Lett. **10,** 011201 (2012)
8. B. Xu, Y. Li, M. Sun, Z. Zhang, X. Dong, Z. Zhang, and S. Jin, Opt. Lett. **37,** 4768 (2012).
9. P. Jia and D. Wang, Chin. Opt. Lett. **11,** 040601 (2013).
10. Y. Zhu, P. Shum, C. Lu, M. B. Lacquet, P. L. Swart, A. A. Chtcherbakov, and S. J. Spammer, Opt. Express **11,** 1918 (2003).
11. W. Zhou, X. Dong, K. Ni, C. C. Chan, and P. Shum, Sensor Actuat. A: Phys. **157,** 15 (2010).
12. T. Guo, A. Ivanov, C. Chen, and J. Albert, Opt. Lett. **33,** 1004 (2008).
13. Y. Huang, T. Guo, C. Lu, and H. Y. Tam, IEEE Photon. Technol. Lett. **22,** 1235 (2010).
14. Y. Guo, D. Zhang, Z. Zhou, L. Xiong, and X. Deng, Chin. Opt. Lett. **11,** 070604 (2013).
15. G. Wild and S. Hinckley, IEEE Sens. J. **8,** 1184 (2008).

16. Y. R. García, J. M. Corres, and J. Goicoechea, J. Sensors **1,** 1 (2010).
17. A. I. Azmi, D. Sen, W. Sheng, J. Canning, and G. Peng, J. Lightwave Technol. **29,** 3453 (2011).
18. Y. N. Zhu, P. Shum, C. Lu, M. B. Lacquet, P. L. Swart, and S. J. Spammer, IEEE Photon. Technol. Lett. **15,** 1437 (2003).
19. X. Guo, Z. Yin, and N. Song, Chin. Opt. Lett. **2,** 393 (2004).
20. L. Su and S. R. Elliott, Opt. Lett. **35,** 1212 (2010).
21. V.Trudel and Y.St-Amant, Appl. Opt. **48,** 4851 (2009).
22. W. B. Spillman, Jr. and R. L. Gravel, Opt. Lett. **5,** 30 (1980).
23. G. A. Rines, Appl. Opt. **20,** 3453 (1981).
24. G. R. Hadley, Opt. Lett. **17,** 1426 (1992).
25. T. Beléndez, C.Neipp, and A. Beléndez, Eur. J. Phys. **23,** 371 (2002).
26. A. V. Oppenheim, A. S. Willsky, and S. H. Nawab, *Signals and Systems* (Tsinghua University Press, Beijing, 1999).